Jeong *et al. Int J Concr Struct Mater* (2025) 19:28
https://doi.org/10.1186/s40069-024-00760-2

International Journal of Concrete Structures and Materials

RESEARCH Open Access

Experimental Study of Interface Shear Transfer of Steel Fiber Reinforced Concrete Members

Daun Jeong[1], Dong-Hee Son[2*], Chang-Sik Choi[1] and Baek-Il Bae[3]

Abstract

This study aimed to evaluate the shear friction strength mechanism of monolithically and separately cast concrete members using steel fiber reinforced concrete (SFRC). To achieve this, a total of 30 push-off tests were conducted with variables such as volume fraction of steel fiber, clamping force of shear-friction reinforcement, and concrete compressive strength. The experimental results showed that the inclusion of steel fibers significantly increased the shear friction strength of monolithically cast concrete. Similarly, the strength improvement in the separately cast specimens was notable with the addition of steel fibers. Notably, as the steel fiber content increased, the concrete contribution also improved, which was attributed to the enhancement of dowel action by the shear-friction reinforcement and the increased tensile strength of the concrete. When comparing the experimental results with current design standards, Eurocode2 provided the most accurate predictions, suggesting that the tensile strength of concrete increased by steel fibers can lead to more precise predictions of shear friction strength.

Keywords Steel fiber reinforced concrete, Shear friction, Precast concrete, Dowel action

1 Introduction

Steel fiber reinforced concrete (SFRC) offers the advantages of high tensile strength and ductility, which help to address some of the inherent weaknesses of conventional concrete (Son et al.). Despite these benefits, the application of SFRC in construction sites faces challenges due to workability issues (ACI 544.14-96, 2002). As an alternative, incorporating SFRC into precast concrete, which can be produced in a controlled factory environment, both resolves the workability problems and allows for the local application of SFRC on-site. This approach enhances both efficiency and the overall performance of the structure (Abbas et al., 2014).

Unlike in reinforced concrete, additional considerations for shear friction are necessary when designing flexural members in precast concrete as illustrated in Fig. 1 (Martin & Perry, 2004). The first case (Fig. 1a) involves bearing at the ends of the flexural members, the second concerns direct shear failure at the precast dapped-end (Fig. 1b), the third case relates to direct shear failure due to the gravity load applied at the member and construction loads on the bracket (Fig. 1c), and the fourth involves horizontal shear failure at the interface (Fig. 1d). Numerous studies (Barragan et al., 2006; Picazo et al., 2021; Soetens & Matthys, 2017) have demonstrated that monolithically cast SFRC is able to improve performance against direct shear. However, research on the interface between precast concrete (PC) elements and cast-in-place concrete (CIP) remains insufficient.

Journal information: ISSN 1976-0485 / eISSN 2234-1315.

*Correspondence:
Dong-Hee Son
son91com@hanyang.ac.kr
[1] Department of Architectural Engineering, Hanyang University, Seoul 04763, Republic of Korea
[2] STRESS Center, Department of Architectural Engineering, Hanyang University, Seoul 04763, Republic of Korea
[3] Department of Digital Architecture and Urban Engineering, Hanyang Cyber University, Seoul 04763, Republic of Korea

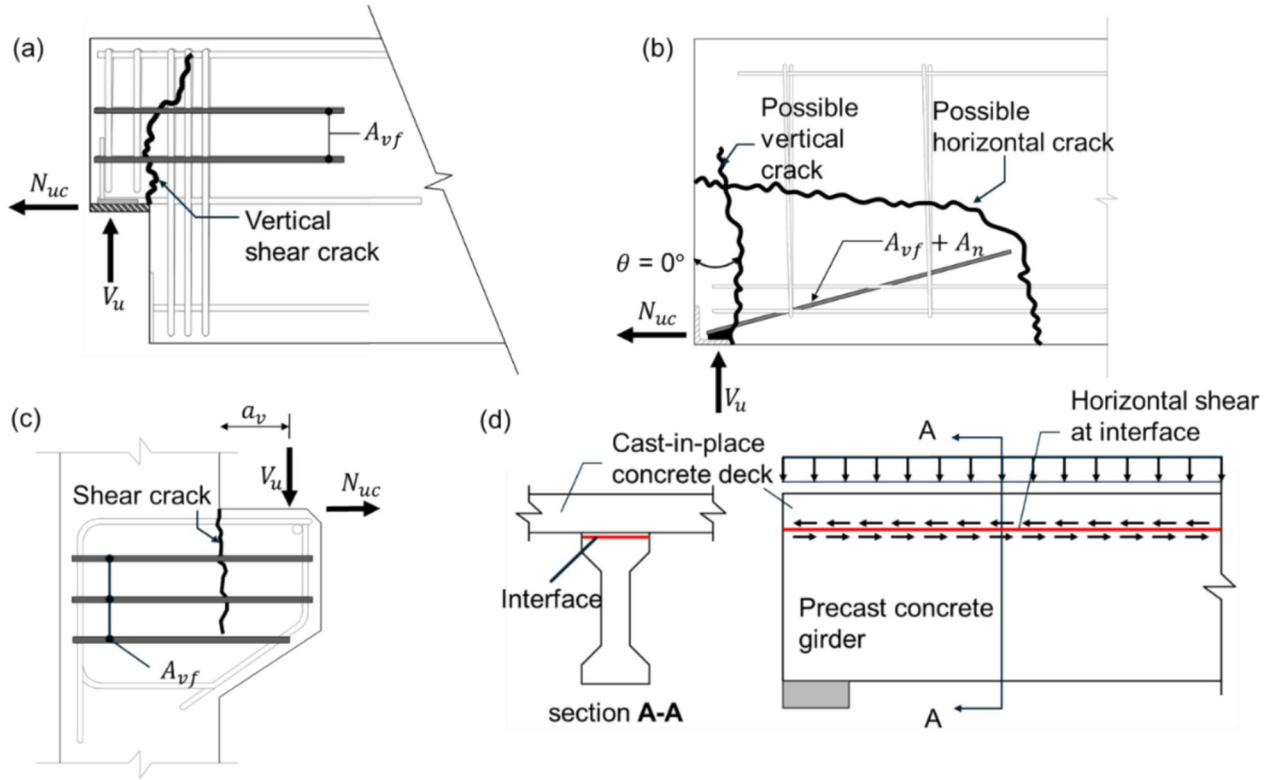

Fig. 1 Shear friction design case of precast concrete members: a dapped-end connection; b bearing region; c corbel; d composite beam

In the case of PC composite beams, horizontal shear forces can occur at the interface, causing the PC beam and CIP concrete to behave separately (Hanson, 1960). To prevent this, sufficient shear-friction reinforcement is placed between the PC elements and CIP concrete, or interface treatments like shear keys are employed to induce monolithic behavior in the separately cast components. Numerous studies have been conducted on the shear transfer mechanism (Birkeland & Birkeland, 1966; Hsu et al., 1987; Kahn & Mitchell, 2002; Loov & Patnaik, 1994; Mast, 1968; Mattock & Hawkins, 1972; Vecchio & Collins, 1986). Birkeland and Birkeland (1966) were the first to simplify this shear transfer mechanism and proposed the shear friction theory. Equations for shear friction strength have been developed through various studies by Mattock and others. These studies revealed that the shear-transfer mechanism resists horizontal shear forces through a combination of aggregate interlock, concrete adhesion, shear friction, and dowel action of the shear-friction reinforcement. These mechanisms are reflected in various design equations according to current design codes.

Therefore, research has been conducted on methods to enhance shear friction strength at interfaces with separate casts using SFRC. Resende et al. (2020) reported that steel fibers increase the contribution of shear strength derived from the dowel action of reinforcement. Zhang et al. (2020) studied shear transfer between SFRC and steel beams, finding that SFRC achieved approximately 20% higher strength compared to conventional concrete. This improvement was attributed to the prevention of concrete crushing by the shear connector. Jang et al. (2017) evaluated the shear friction strength of UHPC based on the condition of the interface. Semendary et al. (2020) conducted a study on shear friction performance at the interface between UHPC and HSC and confirmed that ductility was enhanced by steel fibers. Moreover, these studies have indicated that current standards may have limitations in fully accounting for the effects of steel fibers.

Incorporating steel fibers into PC members is expected both to prevent local failure due to bearing pressure and to delay the failure of CIP concrete and promote composite behavior between PC members and CIP. While numerous studies have been conducted on the shear friction strength of conventional concrete, research on the shear friction strength of separately cast SFRC remains limited. Since steel fibers could potentially replace traditional reinforcement in monolithic casting, this study aims to evaluate the shear friction strength associated

with the inclusion of steel fibers in both monolithically and separately cast concrete. To achieve this, push-off tests were conducted with varying shear-friction reinforcement ratio and volume fraction of steel fiber as main variables.

2 Current Design Code

2.1 ACI 318-19 & KDS 14 20 22

ACI 318-19 and KDS 14 20 22: 2021 use an approach for shear friction design that adjusts the friction coefficient based on the condition of the interface (monolithic or non-monolithic). In this method, only the shear friction contribution of reinforcement is considered, as calculated in Eq. (1). For monolithic casting, a friction coefficient μ of 1.4 λ is applied. When the roughness of the contact surface is approximately 6 mm, a coefficient of 1.0 λ is used. A coefficient of 0.6 λ is applied for cases where new concrete is cast against existing concrete that has not been intentionally roughened.

$$V_n = \mu A_{\mathrm{vf}} f_{\mathrm{yt}}. \tag{1}$$

Here, λ represents the lightweight concrete coefficient, where it is 0.75 for all-lightweight concrete, 0.85 for sand-lightweight concrete, and 1.0 for normal-weight concrete. Linear interpolation from 0.85 to 1 is permitted based on the absolute volume of normal-weight coarse aggregate as a fraction of the total absolute volume of aggregate. A_{vf} is area of shear-friction reinforcement, f_{yt} is specified yield strength of the shear reinforcement.

2.2 Eurocode 2

Eurocode 2 (EC2) considers only the shear stress at the interface for separately cast concrete, rather than for monolithically cast concrete. The shear resistance at the interface can be calculated using Eq. (2), which accounts for the contributions of concrete, reinforcement, and the stress acting perpendicular to the interface. In this calculation, the adhesive bond provided by the concrete is influenced by the tensile strength of the concrete (f_{ctd}). EC2 provides different friction coefficients, c and μ, for concrete and reinforcement, respectively, with these values varying depending on the condition of the interface.

$$v_n = \mathrm{cf}_{\mathrm{ctd}} + \mu\sigma_n + \rho f_{\mathrm{yd}}(\mu \sin\alpha + \cos\alpha) \leq 0.5\mathrm{vf}_{\mathrm{cd}}. \tag{2}$$

Here, f_{ctd} is tensile strength of concrete, σ_n is external stress applied perpendicular to the interface, f_{yd} is yield strength of shear reinforcement, ρ is shear reinforcement ratio, α is angle of shear reinforcement, ν is strength reduction factor ($\nu = 0.6[1 - f_{\mathrm{ck}}/250]$), friction coefficient c and μ follow Table 1:

2.3 fib Model Code 2020

The fib Model Code 2020, like EC2, only considers the shear resistance at the interface between concrete cast at different times, rather than monolithically cast concrete. Unlike EC2, it distinguishes between cases with and without reinforcement. In the absence of reinforcement, the shear resistance is calculated similarly to EC2, accounting for the contribution from the adhesive bond of concrete and the compressive stress acting perpendicular to the interface, as shown in Eq. (3). Here, the adhesive bond provided by the concrete is proportional to the tensile strength of the concrete. The coefficient for the adhesive bond (c_a) differs from that in EC2.

In the case with reinforcement, the shear friction strength is calculated using Eq. (4), which involves the superposition of interlocking, shear friction, and dowel action, based on Randl's research (Randl,). The first term represents interlocking, the second term shear friction, and the final term accounts for the dowel action of the shear-friction reinforcement. Unlike Eq. (3), the shear resistance due to adhesive bond and interlocking is proportional to the cube root of the concrete compressive strength.

$$\text{Interface without reinforcement:} \tau_{\mathrm{Rdi}} = c_a f_{\mathrm{ctd}} + \mu\sigma_n \leq 0.25 f_{\mathrm{cd}}. \tag{3}$$

$$\text{Interface intersected by dowels or reinforcement:} \tau_{\mathrm{Rdi}} = c_r f_{\mathrm{ck}}^{1/3} + \mu\left(\rho\kappa_1 f_y + \sigma_n\right) + \kappa_1 \rho\sqrt{f_y f_{\mathrm{cc}}} \leq \beta_c f_{\mathrm{cc}}. \tag{4}$$

Table 1 Value of c and μ depending on roughness of interface according to Eurocode2

Classification of surface condition	c	μ
Very smooth: a surface cast against steel, plastic or specially prepared wooden molds	0.25	0.5
Smooth: a slip-formed or extruded surface, or a free surface left without further treatment after vibration	0.35	0.6
Rough: a surface with at least 3 mm roughness at about 40 mm spacing, achieved by raking, exposing of aggregate or other methods giving an equivalent behavior	0.45	0.7
Indented: a surface with indentations	0.50	0.9

Here, c_a is the coefficient for the adhesive bond, c_r is the coefficient for aggregate interlock effects at rough interfaces, κ_1 is the interaction coefficient for tensile force activated in the reinforcement or the dowels, κ_2 is the interaction coefficient for flexural resistance, μ is the friction coefficient, ρ is the reinforcement ratio of the reinforcing steel crossing the interface, is the (lowest expected) compressive stress resulting from an eventual normal force acting on the interface, β_c is the coefficient for the strength of the compression strut. The values of each coefficient are given in Table 2.

2.4 AASHTO LRFD

In AASHTO LRFD, a design equation similar to that of ACI 318-19 is used, but it considers the effects of cohesion and/or aggregate interlock, as calculated in Eq. (5). Like ACI 318-19, it considers both monolithic and separate casting conditions, providing a cohesion factor c and a friction factor μ based on the condition of the interface. Notably, c, unlike in EC2 and fib Model Code 2020, has a fixed stress value depending on the interface condition and is independent of the concrete strength. With the surface intentionally roughened to an amplitude of 6 mm, c is 1.7 MPa and μ is 1.0. For concrete placed against a clean concrete surface, but not intentionally roughened, c is 0.52 MPa and μ is 0.6:

$$v_{\mathrm{ni}} = cA_{\mathrm{cv}} + \mu\left(A_{\mathrm{vf}}f_y + P_c\right) \le \min\left(K_1 f_c', K_2\right). \quad (5)$$

2.5 JSCE

In JSCE standard specification for concrete structures design, the shear friction strength is calculated using Eqs. (6) to (9), which account for the shear resistance provided by the concrete (Eq. (7)) and the resistance from the reinforcement and the compressive force acting perpendicular to the interface (Eq. (8)). In JSCE, the contribution of concrete to shear friction is considered based on its compressive strength. Additionally, it considers the fact that as the shear-friction reinforcement ratio increases, the clamping force acting perpendicular to the concrete shear plane diminishes before all the reinforcement yields:

$$v_{\mathrm{cwd}} = \tau_c + p\tau_s \sin^2\theta - \alpha p f_{\mathrm{yd}} \sin\theta\cos\theta, \quad (6)$$

$$\tau_c = \mu f_{\mathrm{cd}}^b \left(\alpha p f_{\mathrm{yd}} - \sigma_{\mathrm{nd}}\right)^{1-b}, \quad (7)$$

$$\tau_s = 0.08 f_{\mathrm{yd}}/\alpha, \quad (8)$$

$$\alpha = 0.75\left\{1 - 10\left(p - 1.7\sigma_{\mathrm{nd}}/f_{\mathrm{yd}}\right)\right\}. \quad (9)$$

Here, σ_{nd} is average normal stress acting on the shear plane, p is the reinforcement ratio along the shear plane, θ is angle between shear plane and reinforcement, b is coefficient representing configuration of planes and ranging between 0 and 1, μ is average coefficient of friction for solid-to-solid contact (0.45), f_{cd} is concrete compressive strength, f_{yd} is yield strength of shear friction reinforcement.

3 Experimental Plan

3.1 Test Specimens Design

The objective of this study is to evaluate the shear friction strength for the design of precast concrete members. Accordingly, a total of 30 push-off tests were conducted to evaluate the shear friction strength of both monolithically and non-monolithically cast steel fiber-reinforced concrete. Design standards such as ACI 318-19 consider the clamping force of shear-friction reinforcement as a key design parameter. Furthermore, standards like EC 2 and MC 2020 consider the compressive and tensile strength of concrete to reflect the effects of interlocking and adhesive bond. As the tensile strength of concrete increases with the inclusion of steel fibers, the effects of interlocking and adhesive bonds are expected to increase accordingly.

Therefore, the main experimental variables include the casting condition (monolithic and non-monolithic), the clamping force ($\rho_v f_{\mathrm{yt}}$) based on the shear-friction reinforcement ratio (ρ_v), the volume fraction of steel fiber (V_f), and the compressive strength. For the monolithic specimens, experiments were conducted without reinforcement to evaluate the potential of replacing reinforcement with steel fibers. In the case of the non-monolithic

Table 2 Coefficients for different surface roughness according to MC2020

Surface roughness	c_r	κ_1	κ_2	β_c	μ	
					$f_{ck} \ge 20$	$f_{ck} \ge 35$
Very rough	0.2	0.5	0.9	0.5	0.8	1.0
Rough	0.1	0.5	0.9	0.5	0.7	
Smooth	0	0.5	1.1	0.4	0.6	
Very smooth	0	0	1.5	0.3	0.5	

specimens, the clamping force of the shear-friction reinforcement (with a specified yield strength of 400 MPa) was set to 0, 1.9, 3.8, and 5.7 MPa to assess the effects on the shear friction strength of separately cast steel fiber-reinforced concrete in each range.

According to ACI 544.1R-96, balling of fibers is likely to occur when the steel fiber content exceeds 1.5 to 2.0%. In a study by Kal et al. (2010), specimens with a 2% steel fiber content showed lower strength compared to those with 1% and 1.5% due to the balling of fibers. Therefore, in this study, the volume fraction of steel fiber for the 40 MPa concrete, representing PC, was set to 0% and 1%, while for the 24 MPa concrete, representing CIP, it was set to 0%, 1%, and 1.5%. The experimental variables are summarized in Table 3. The first part of the specimen name indicates the casting type and the number of shear-friction reinforcements. The second and third parts represent the steel fiber content for 40 MPa ($f_{ck,PC}$) and 24 MPa ($f_{ck,CIP}$) concrete, respectively. The fourth part (a, b, c) is used to differentiate identical specimens.

The dimensions of all specimens were 700 mm × 400 mm × 150 mm, and the shear plane measured 240 mm × 150 mm, resulting in a shear surface area of 36,000 mm2. The shear-friction reinforcement was sufficiently anchored with hooks to ensure yielding. The specimen details are shown in Fig. 2. First, 40 MPa concrete was cast, and following the guidelines of ACI 318-19 and KDS, the interface was cleaned to remove laitance, and the surface was roughened to approximately 6 mm. A week later, 24 MPa concrete was cast on the opposite side for the second pour.

3.2 Material Properties

For the material strength test of the concrete, cylindrical specimens with dimensions of ϕ 100 mm × 200 mm were prepared according to KS F 2403 and cured under

Table 3 Specimens detail

No	Specimen ID	Shear plane (mm)	$\rho_v f_{yt}$ (MPa)	f_{ck} (MPa)	Interface	$V_{f,PC}$ (%)	$V_{f,CIP}$ (%)
1	M-24-0-a	240 x 150	0	24 (CIP)	–	–	0
2	M-24-0-b						
3	M-24-1-a						1
4	M-24-1-b						
5	M-24-1.5						1.5
6	M-40-0-a			40 (PC)			0
7	M-40-0-b						
8	M-40-1-a						1
9	M-40-1-b						
10	S0-0-0-a			24 (CIP) 40 (PC)	Non-monolithic (cast in difference time)	0	0
11	S0-0-0-b						
12	S0-0-0-c						
13	S0-1-0-a					1	0
14	S0-1-0-b						
15	S0-1-0-c						
16	S0-1-1-a					1	1
17	S0-1-1-b						
18	S0-1-1-c						
19	S1-0-0		1.9 (1-D10)			0	0
20	S1-1-0					1	
21	S1-1-1						1
22	S1-1-1.5						1.5
23	S2-0-0		3.8 (2-D10)			0	0
24	S2-1-0					1	
25	S2-1-1						1
26	S2-1-1.5						1.5
27	S3-0-0		5.7 (3-D10)			0	0
28	S3-1-0					1	
29	S3-1-1						1
30	S3-1-1.5						1.5

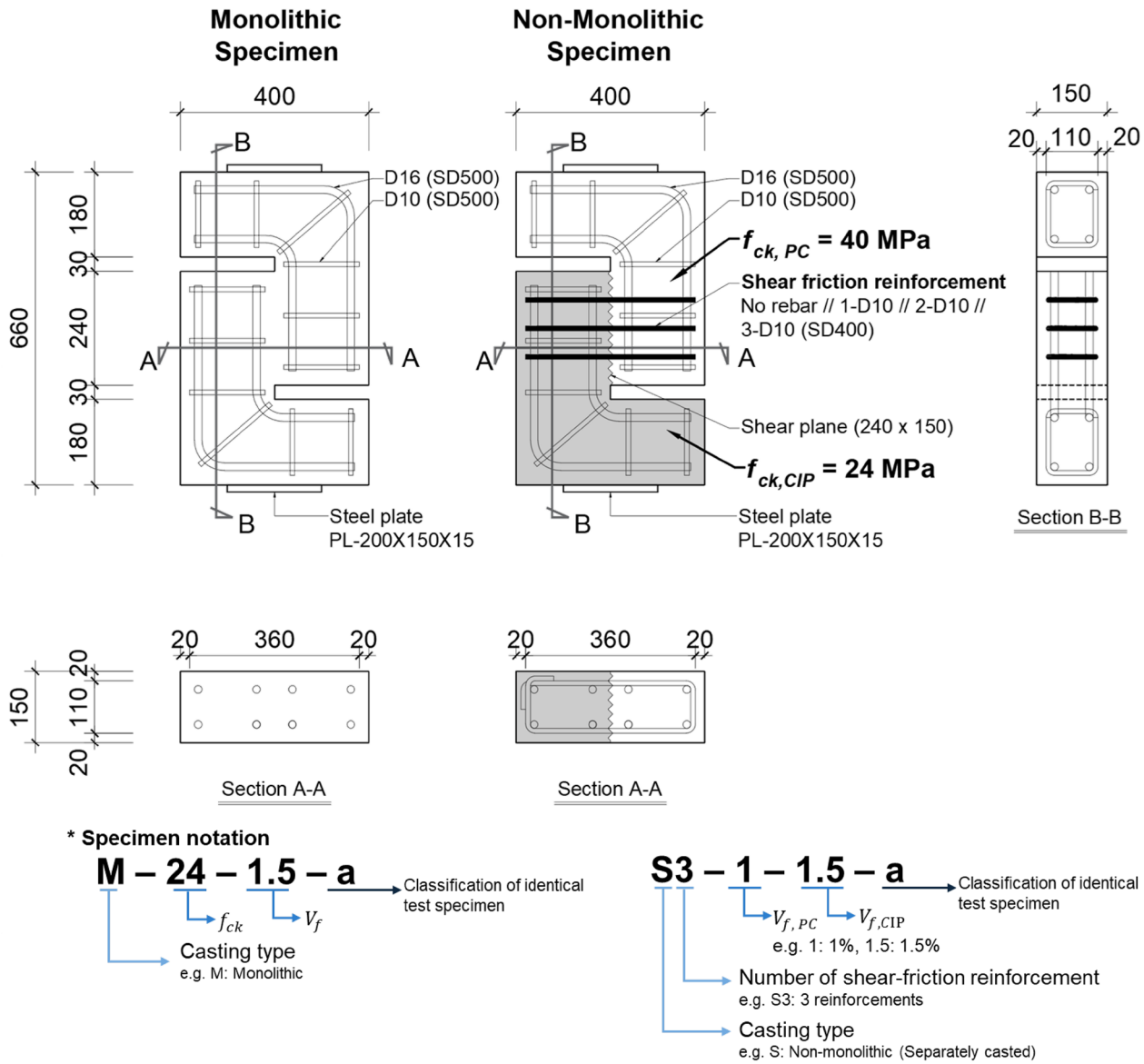

Fig. 2 Push-off specimen details (unit: mm)

the same conditions as the test specimens. The compressive strength of the concrete and the mix proportion according to the steel fiber content are shown in Table 4. The steel fibers used for the test specimens were hooked-end type fibers with a diameter of 0.5 mm and a length of 30 mm. Compressive strength and splitting tensile strength tests were performed on the cylindrical concrete specimens in accordance with KS

Table 4 Mix proportions of concrete

Specified strength	W/C (%)	S/a (%)	Unit weight (kg/m^3)				
			W	C	S	G	Ad
40	30.1	42.8	164	463	693	927	4.4
24	48.4	47.9	165	290	863	938	2.7

W/C, water–cement ratio; S/a, sand–aggregate ratio; W, water; C, cement; S, fine aggregate; G, coarse aggregate; Ad, admixture

F 2405 and KS F 2423. The flexural tensile strength test was conducted using prism specimens measuring 100 mm × 100 mm × 400 mm, with a notch at the center to measure the crack mouth opening displacement (CMOD).

The results of the concrete material tests are shown in Table 5. In the splitting tensile strength test, when 1% steel fiber was added, the splitting tensile strength increased by 9.4% in 40 MPa concrete and by 11.6% in 24 MPa concrete. For flexural tensile strength, in the case of $f_{ck,\,PC}$ = 40 MPa concrete, a 1% steel fiber content resulted in a 2.06-fold increase, and a 1.5% content led to a 2.38-fold increase. For $f_{ck,\,CIP}$ = 24 MPa concrete, a 1% fiber content resulted in approximately a 1.81-fold increase. To evaluate the mechanical properties of the shear-friction reinforcement, a tensile strength test was performed in accordance with KS B 0802, and the yield strength of the SD400 D10 shear-friction reinforcement was 471.6 MPa.

3.3 Material Properties

In this study, a direct shear test was performed using a 2,000-kN capacity universal testing machine (UTM). The 40 MPa concrete was positioned at the top, and steel plates measuring 200 mm × 150 mm × 15 mm were placed at both the top and bottom of the specimen. The loading rate was set to 0.1 mm/min until the specimen reached its maximum load. The test was terminated after the shear-friction reinforcement yielded and the load dropped to less than half of the maximum load. The strain and displacement of the specimens were measured as shown in Fig. 3a and b.

First, strain gauges were attached to each shear-friction reinforcement to measure the strain and identify the yield point. Harries et al. (2012) measured strain 75 mm away

Table 5 Mechanical properties of concrete

Specified strength	V_f (%)	f_c' (MPa)	f_{sp} (MPa)	f_r (MPa)	f_{R1} (MPa)	f_{R2} (MPa)	f_{R3} (MPa)
40	0	48.14	3.43	4.57	–	–	–
	1	36.42	3.76	8.29	7.42	6.60	7.62
24	0	36.19	3.17	4.85	–	–	–
	1	31.53	3.54	10.00	8.96	6.98	5.84
	1.5	35.38	4.06	11.53	10.53	9.94	7.38

V_f, volume fraction of steel fiber; f_c', concrete compressive strength; f_{sp}, splitting tensile strength; f_r, flexural strength of concrete; $f_{R,1,2,3}$, residual flexural tensile strength corresponding to CMOD = 0.5, 1.5, 2.5, and 3.5 mm, respectively

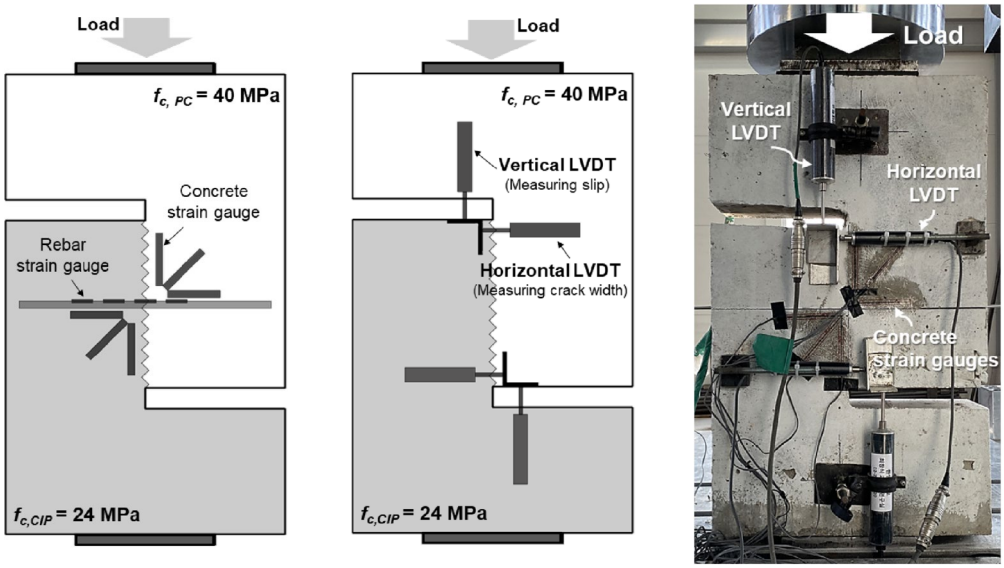

(a) Gauge plan (b) LVDT plan (c) Test setup

Fig. 3 Push-off test configuration

from the shear plane to prevent damage to the gauges. Additionally, the strain difference between the shear plane and the measurement location becomes minimal as the concrete deteriorates during testing. In this study, gauges were attached across the shear plane, and to prevent gauge damage and identify areas where strain was concentrated, additional gauges were placed 45 mm and 90 mm away from the shear plane.

Secondly, strain gauges were attached to the concrete at three angles, 10 mm away from the shear plane, to measure the shear strain in the concrete. Gauges were installed on both the 40 MPa and 24 MPa concrete, with a total of six strain gauges per specimen. Lastly, a vertical LVDT was installed to measure the slip of the specimen, and a horizontal LVDT was used to measure the crack width at the shear plane. The actual setup of the specimen is shown in Fig. 3c.

4 Experimental Results

4.1 Shear Friction Strength

The crack width, slip, and strain of the shear-friction reinforcement at the points of initial cracking and maximum load are presented in Table 6. The crack width (w_u) was measured using the horizontal LVDT installed on the specimen, while the slip (δ_{cr}, δ_u) was measured using the vertical LVDT. The strain of the shear-friction reinforcement was calculated as the average of the gauge readings taken from the center of each reinforcement bar. The

Table 6 Push-off test results

No	Specimen ID	Cracking load				Ultimate load				
		V_{cr} (kN)	τ_{cr} (MPa)	δ_{cr} (mm)	$\varepsilon_{s,cr}$ (μ)	V_u (kN)	τ_u (MPa)	δ_u (mm)	w_u (mm)	$\varepsilon_{s,u}$ (μ)
1	M-24-0-a	10.4	0.28	0.01	–	180.36	5.01	0.353	0.044	
2	M-24-0-b	13.92	0.38	0.01		186.18	5.17	0.360	0.044	
3	M-24-1-a	16.58	0.46	0.02		238.46	6.62	0.763	0.455	
4	M-24-1-b	10.16	0.28	0.01		213.14	5.92	0.655	0.376	
5	M-24-1.5	9.98	0.28	0.01		230.96	6.42	0.663	0.406	
6	M-40-0-a	14.54	0.40	0.06		181.46	5.04	0.390	0.045	
7	M-40-0-b	11.02	0.31	0.01		156.44	4.35	0.305	0.027	
8	M-40-1-a	9.14	0.25	0.01		204.58	5.68	0.433	0.199	
9	M-40-1-b	13.48	0.37	0.02		204.58	5.68	0.605	0.302	
10	S0-0-0-a	13.38	0.37	0.01		81.72	2.27	0.145	0.025	
11	S0-0-0-b	8.86	0.24	0.01		85.26	2.37	0.120	0.004	
12	S0-0-0-c	13.62	0.37	0.01		108.16	3.00	0.175	0.012	
13	S0-1-0-a	7.8	0.21	0.01		87.98	2.44	0.105	0.019	
14	S0-1-0-b	6.22	0.17	0.01		110.90	3.08	0.215	0.038	
15	S0-1-0-c	8.8	0.24	0.02		109.62	3.05	0.230	0.006	
16	S0-1-1-a	8.94	0.25	0.01		123.18	3.42	0.100	0.007	
17	S0-1-1-b	8.76	0.24	0.01		100.52	2.79	0.175	0.020	
18	S0-1-1-c	10.82	0.30	0.03		108.34	3.01	0.265	0.014	
19	S1-0-0	105.76	2.93	0.17	105	87.60	2.43	1.325	0.431	1628
20	S1-1-0	91.74	2.54	0.09	99	110.14	3.06	0.145	0.164	535
21	S1-1-1	114.28	3.17	0.14	182	127.92	3.55	0.255	0.147	1108
22	S1-1-1.5	66.84	1.85	0.03	135	72.12	2.00	1.630	0.691	2051
23	S2-0-0	90.66	2.51	0.22	82	120.08	3.34	3.393	0.663	1150
24	S2-1-0	57.58	2.24	0.07	99	100.66	2.80	0.190	0.085	541
25	S2-1-1	53.58	1.48	0.08	34	154.08	4.28	0.348	0.123	488
26	S2-1-1.5	95.62	2.65	0.12	144	107.24	2.98	0.193	0.066	595
27	S3-0-0	107.44	2.98	0.17	115	150.36	4.18	0.318	0.080	396
28	S3-1-0	120.52	3.34	0.17	92	228.42	6.35	0.770	0.239	940
29	S3-1-1	131.02	3.63	0.15	92	192.86	5.36	0.688	0.230	781
30	S3-1-1.5	38.16	1.06	0.04	34	191.74	5.33	19.120	2.394	1289

V_{cr}, cracking load; τ_{cr}, cracking stress; δ_{cr}, displacement at first crack; $\varepsilon_{s,cr}$, rebar strain at first crack; V_u, maximum load; τ_u, maximum shear stress; δ_u, displacement at V_u; w_u, crack width at V_u; $\varepsilon_{s,u}$, rebar strain at V_u

shear stress was computed by dividing the applied load by the shear plane area. The cracking load was defined as the point where the slope of the shear stress–crack width relationship sharply decreases or where the strain in the reinforcement at the interface changes abruptly. In most specimens, these two points occurred almost simultaneously.

4.1.1 Monolithic and Non-monolithic Specimen Without Shear Friction Reinforcements

The load–displacement and load–crack width relationships for the monolithically cast specimens are shown in Fig. 4a and b, respectively. Graphs were not presented for the specimens without reinforcement and cast separately, as they failed immediately after reaching the maximum strength. The experimental results showed that specimens without steel fibers failed immediately after reaching the maximum strength, whereas both strength and deformation capacity improved with the incorporation of steel fibers.

EC2 and MC2020 report that as the tensile strength of concrete increases, the contributions of aggregate interlocking and adhesion bond to shear friction also increase. However, when comparing the strengths of M-40-1 and M-24-1, it was observed that M-24-1 had a slightly higher strength. Therefore, it was necessary to examine how the material test results affected the push-off test. In this regard, the shear stress at the shear plane as tensile

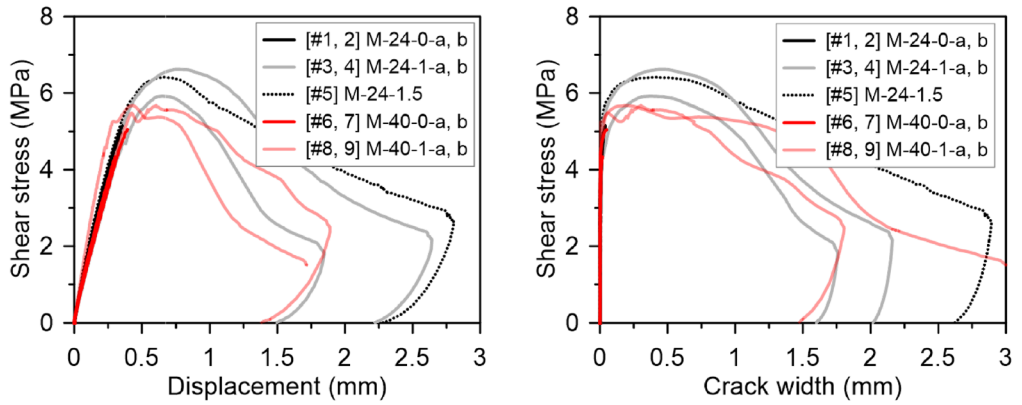

Fig. 4 Load–displacement and crack width relationship of monolithic series

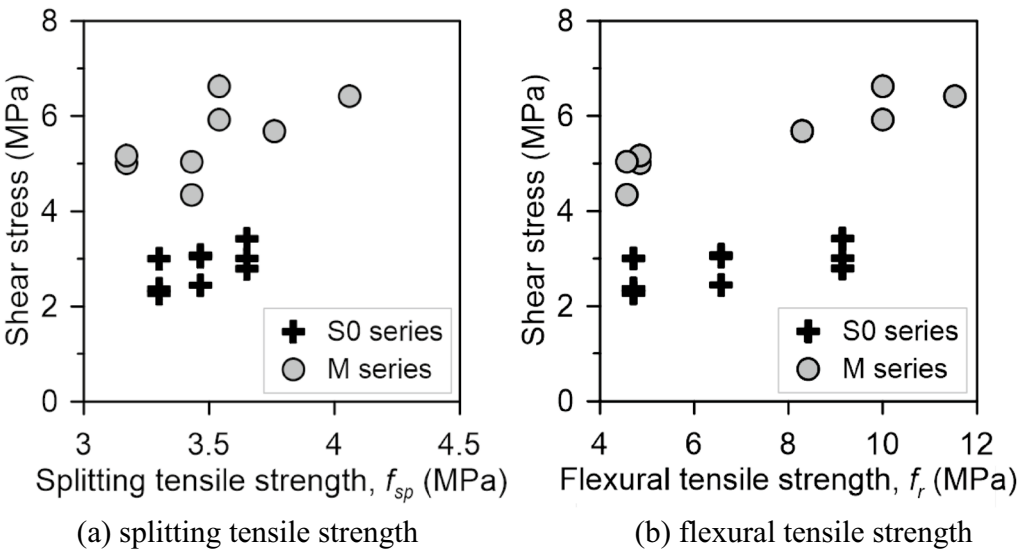

Fig. 5 Shear stress with concrete tensile strength

strength increased was evaluated and is presented in Fig. 5. In this evaluation, the S0 series (non-monolithic) used the average tensile strength of both types of concrete for comparison. The results showed that with an increase in tensile strength, both monolithically cast specimens (M series) and non-monolithic cast specimens (S0 series) exhibited a corresponding increase in splitting tensile strength and flexural tensile strength.

4.1.2 Non-monolithic Specimens with Shear Friction Reinforcements

The load–crack width relationships for the separately cast specimens are shown in Fig. 6. After reaching the maximum strength, the load tended to decrease as the effects of aggregate interlock and concrete adhesion diminished. In the S1 series, the load did not increase further and remained constant. However, as the reinforcement ratio increased, the load in the specimens decreased after reaching maximum strength but then increased again.

In the S1 series, after the first crack occurred, stiffness decreased rapidly, resulting in a small difference between the strength at first cracking and the maximum strength. As the reinforcement ratio increased, the difference between the first crack strength and maximum strength also grew. Additionally, with the inclusion of steel fibers, both the first crack strength and stiffness increased.

In most specimens, the shear-friction reinforcement yielded after the maximum strength was reached. In the S2-1-0 and S3-1-0 specimens, the shear-friction reinforcement yielded before reaching the maximum strength. However, both specimens exhibited similar trends, as they experienced a decrease in strength after initially reaching the peak strength, before ultimately achieving the maximum strength. Therefore, when accounting for the contribution of reinforcement in shear friction, it is necessary to consider the combined action of concrete and reinforcement rather than relying solely on the yield strength of the reinforcement. In the case of the S3-1-1.5 specimen, the strength continued to increase after the reinforcement yielded, and the test was terminated before the specimen could reach its maximum strength. Overall, the experimental results indicate that, except for the 1–1.5 series, the strength increased with the inclusion of steel fibers. This effect was found to be more pronounced as the reinforcement ratio increased.

The changes in shear stress corresponding to variations in clamping force, splitting tensile strength, and flexural tensile strength are shown in Fig. 7. For the S1

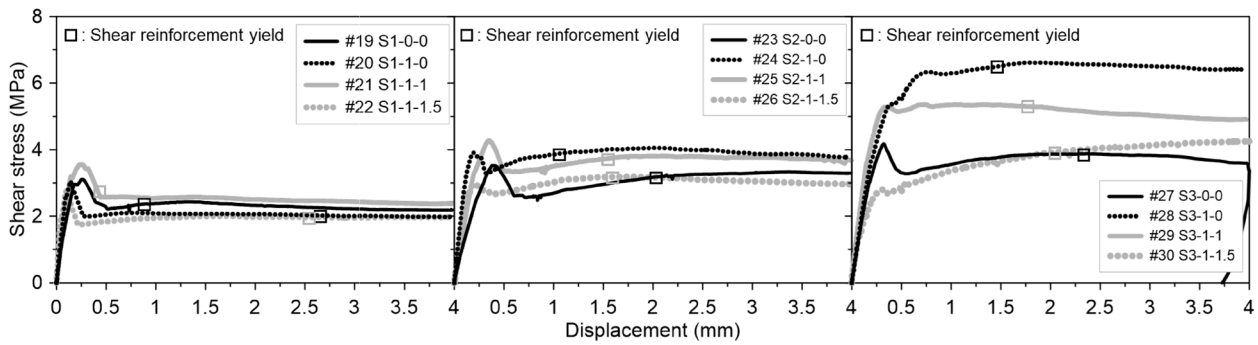

(a) Shear stress-displacement relationship

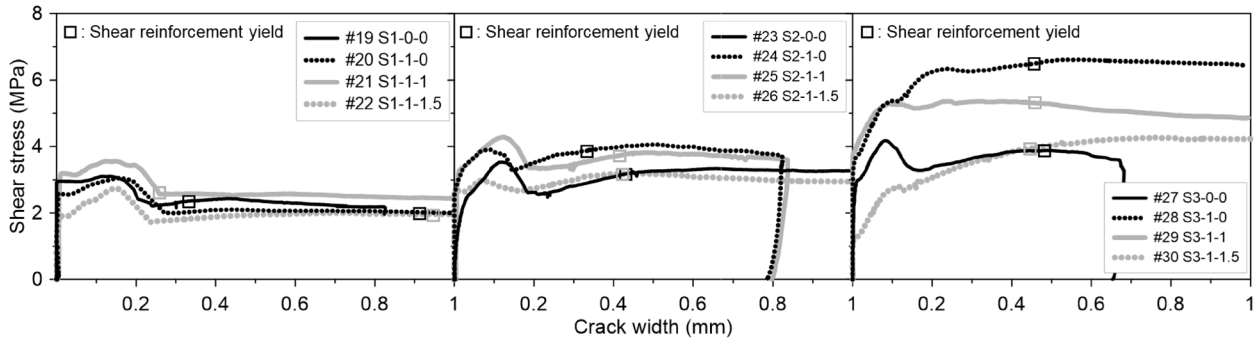

(b) Shear stress-crack width relationship

Fig. 6 Shear stress with displacement and crack width

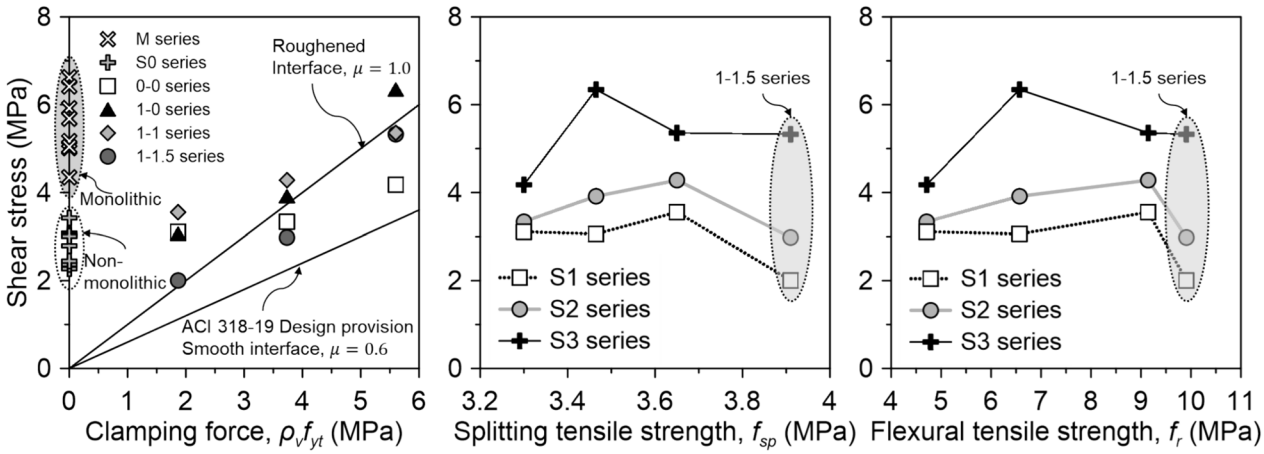

Fig. 7 Shear stress with concrete tensile strength

series, the difference in strength due to the inclusion of steel fibers was not significant. However, for the S2 and S3 series, the maximum strength increased with the inclusion of steel fibers, with the S3 series showing a more pronounced increase in strength compared to the S2 series. As the reinforcement ratio increased, the rate of strength increased due to the incorporation of steel fibers became more pronounced. When comparing these strengths to the monolithic specimens, the S3 series exhibited a similar level of performance.

For shear stress based on splitting tensile strength and flexural tensile strength, all specimens except for the 1–1.5 series showed an increase in shear stress with the addition of steel fibers and an increase in average tensile strength. This matches with previous study (Sagi et al., 2022), which indicated that the improvement in shear strength at 1.5% fiber content is not as significant compared to 0% or 1%. This may be attributed to the possibility of fiber ball effect at higher content levels, which could lead to a reduction in strength (Kal et al., 2010). Notably, the shear strength of the S3 series increased significantly compared to the S2 series. This is likely due both to the increased contribution from interlocking and to the greater effect of SFRC on the dowel action of the reinforcement as the reinforcement ratio increased.

It appears that the roughened finish was not perfectly achieved when comparing the shear stress to the nominal shear stress from ACI 318-19 based on surface treatment methods. This is likely due to the fact that the work was done manually, which is consistent with previous study (Lee et al., 2019), where even with roughened finishes, the strength was lower than the nominal value. Therefore, this study considered both cases. As a result, all specimens achieved at least the friction coefficient for a smooth interface, but some specimens did not meet the friction coefficient for a roughened interface.

4.2 Shear Strain of Concrete

To establish a method for evaluating the contribution of concrete when calculating the shear friction strength of separately cast concrete, the shear strain measured by the concrete gauges attached to the CIP and PC parts was assessed. Shear strain can be calculated using the three attached concrete gauges, as shown in Fig. 8, and is determined by Eqs. (10) and (11):

$$\varepsilon_a = \varepsilon_x \cos^2 \theta_a + \varepsilon_y \sin^2 \theta_a + \gamma_{xy} \sin \theta_a \cos \theta_a, \quad (10)$$

$$\gamma_{xy} = 2\varepsilon_a - \varepsilon_x - \varepsilon_y. \quad (11)$$

To compare the effect of steel fibers, the specimens were divided into the 0–0 series and 1–1 series, as shown in Fig. 9, to observe the changes in shear strain due to the inclusion of steel fibers.

The results showed that, although the CIP ($f_{ck} = 24$ MPa) was expected to exhibit greater shear strain due to its lower material strength and resulting stiffness difference, some cases (#19, #21, #24 in Fig. 9) revealed greater shear strain in the PC part ($f_{ck} = 40$ MPa). Additionally, both parts of the separately cast sections deformed together in terms of shear strain up until the point of maximum strength. Therefore, the earlier assumption of using the average strength of both concretes for strength comparison appears to be valid.

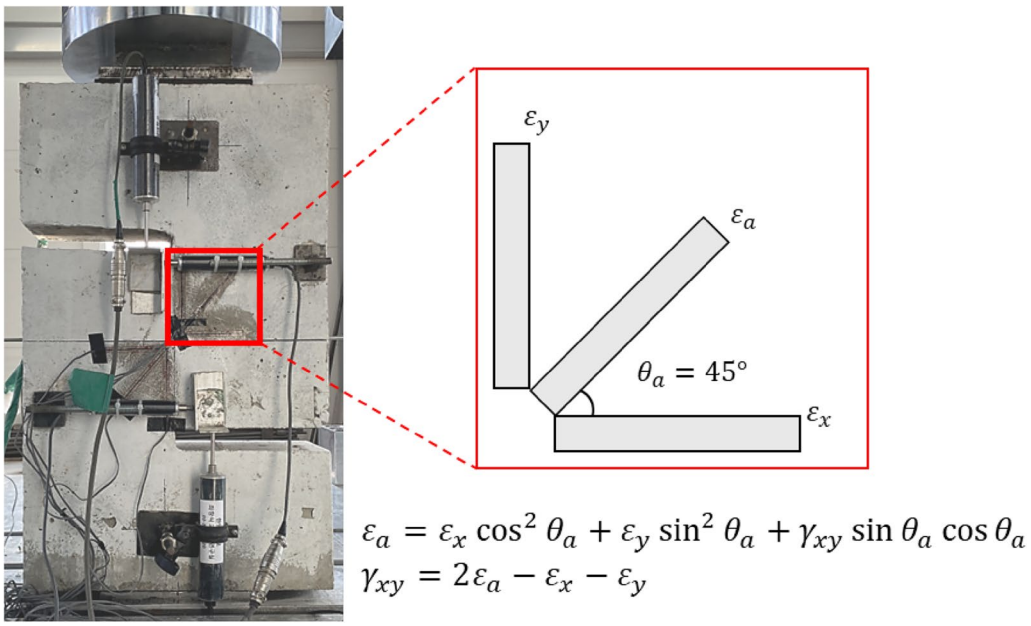

Fig. 8 Measurement of shear strain by concrete strain gauge

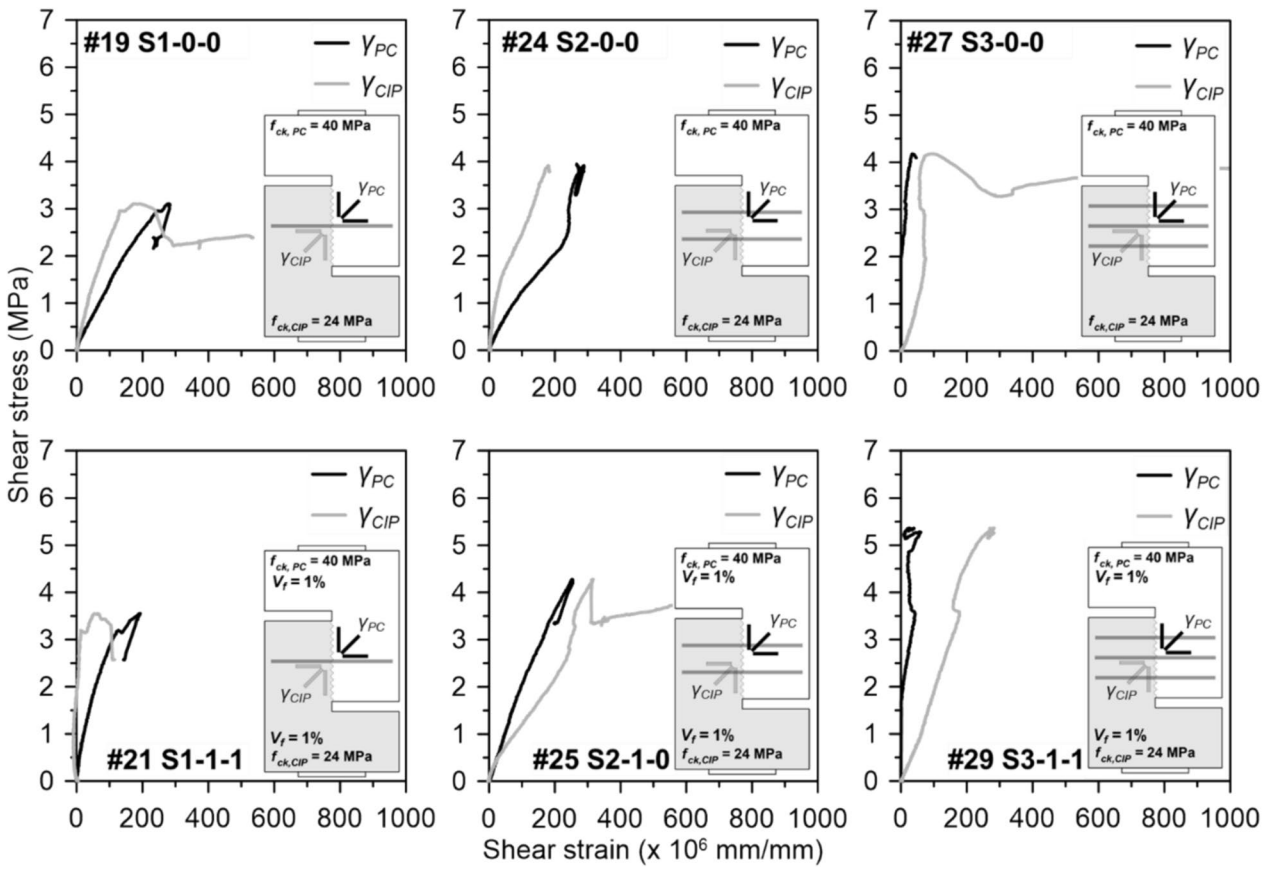

Fig. 9 Shear strain of SFRC specimens

4.3 Concrete Contribution

In the studies by Harries et al. (2012) and Semendary et al. (2020), the shear friction behavior was analyzed by separating the contributions of the concrete and the reinforcement in accordance with the shear transfer mechanism presented by AASHTO LRFD. The concrete's contribution to shear friction, v_c, can be evaluated by subtracting the contribution of the shear-friction reinforcement, v_s, from the total shear friction strength, v_u, as shown in Eq. (12):

$$v_c = v_u - v_s. \tag{12}$$

In Eq. (12), the contribution of the shear-friction reinforcement was calculated by determining the shear force resisted by the reinforcement. This was done by multiplying the friction coefficient for roughened surfaces (μ), the average strain in the reinforcement at the interface (ε_s), the modulus of elasticity of the reinforcement (E_s), and the cross-sectional area of the shear-friction reinforcement (A_{vf}). The resulting shear force was then divided by the area of the shear plane (A_{cv}) to obtain the average shear stress resisted at the interface, as shown in Eq. (13):

$$v_s = \mu \varepsilon_s E_s A_{vf} / A_{cv}. \tag{13}$$

As mentioned in Fig. 7, the actual friction coefficient is expected to range between 0.6 and 1.0. However, to compare behavior, the friction coefficient μ was set to 1.0, consistent with previous studies. The shear friction

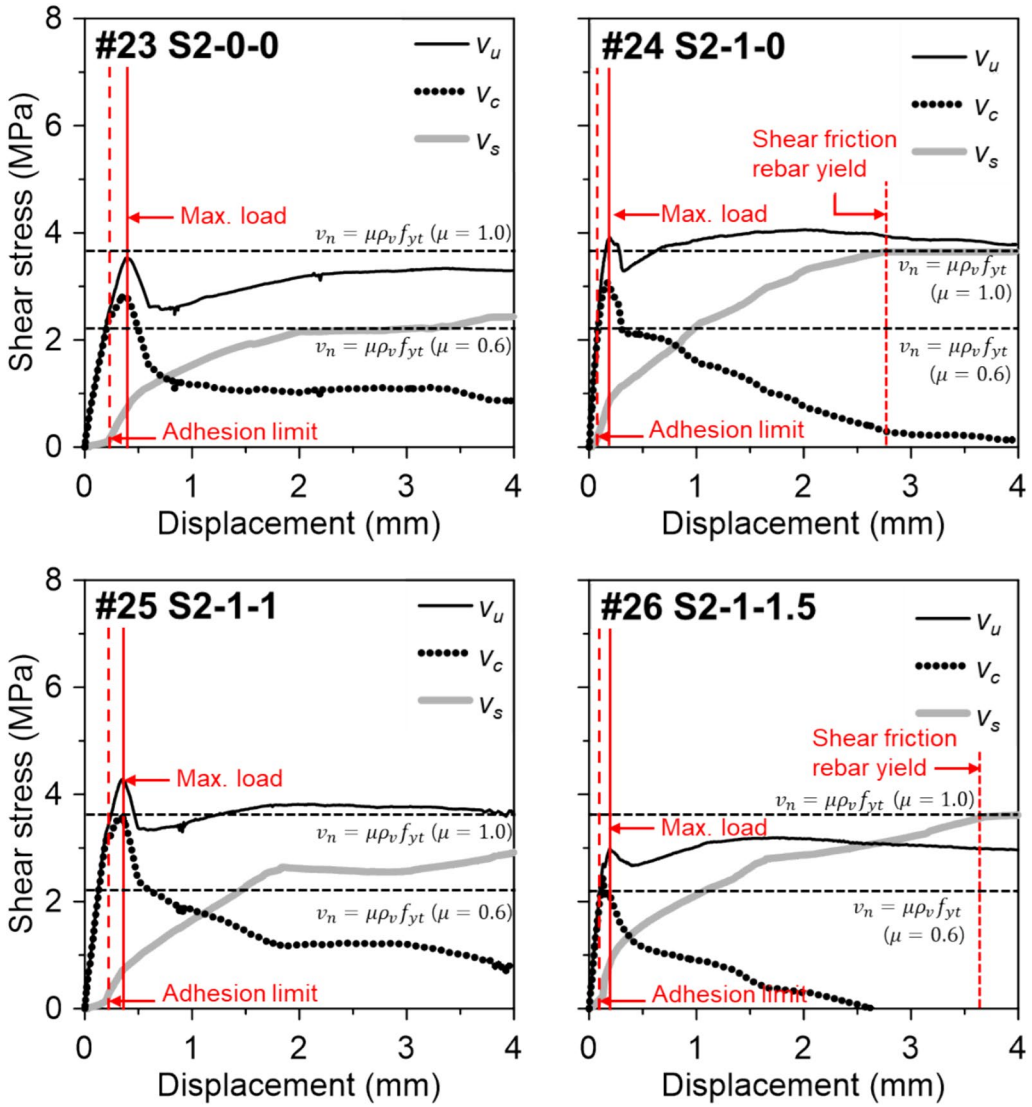

Fig. 10 Components of shear friction behavior

behavior according to Eqs. (12) and (13) is illustrated in Fig. 10, where the shear friction behavior of the S2 Series is shown, focusing on the changes in steel fiber content.

In the adhesion limit states, the concrete primarily resisted the shear friction. After the adhesion limit was exceeded and cracking occurred, the reinforcement began to resist the shear friction. At the point of maximum strength, the reinforcement had not yet yielded, which differs somewhat from the shear friction mechanism presented in ACI 318-19 or AASHTO LRFD. Upon closer examination, the adhesion provided by the concrete appeared to decrease after the adhesion limit, while a combination of dowel action and shear friction by the reinforcement took over. Additionally, the contribution of each mechanism varied as slip increased.

The changes in the contribution of concrete due to the incorporation of steel fibers are shown in Fig. 11. In most cases, specimens with 1% steel fiber in both 40 MPa and 24 MPa concrete had the highest concrete contribution. The concrete contribution ranged from 1.19 to 3.34 MPa, accounting for approximately 41.18% to 90.31% of the maximum shear stress. Similar to the findings in Fig. 7, the increase in shear friction strength appears to be due to the rise in tensile strength resulting from the incorporation of steel fibers. This is likely because the increase is more related to the enhancement of concrete contribution by the steel fiber.

Furthermore, it can be observed that an increase in the amount of reinforcement allows steel fibers to resist more effectively. As seen in the 1–1.5 series, while the strength decreased in specimens S1 and S2, it did not decrease but rather remained stable in specimen S3, further validating this observation. At lower reinforcement ratios, the maximum strength is influenced more by the interlocking effect, but as the reinforcement ratio increases, the influence of concrete becomes more significant.

4.4 Strain Distribution of Shear Friction Rebar

To observe the changes in strain of the reinforcement at different load stages, gauges attached to the shear-friction reinforcement were checked as shown in Fig. 12. Since the CIP portion has a compressive strength of 24 MPa, gauges were attached at distances of 45 mm and 90 mm from the interface to further monitor the strain in the reinforcement.

The gauge measurement results are presented in Fig. 13. As with the previous experimental results, most specimens did not yield at the point of maximum strength. Despite the increase in the number of reinforcement bars, the strain in the CIP part was greater than the

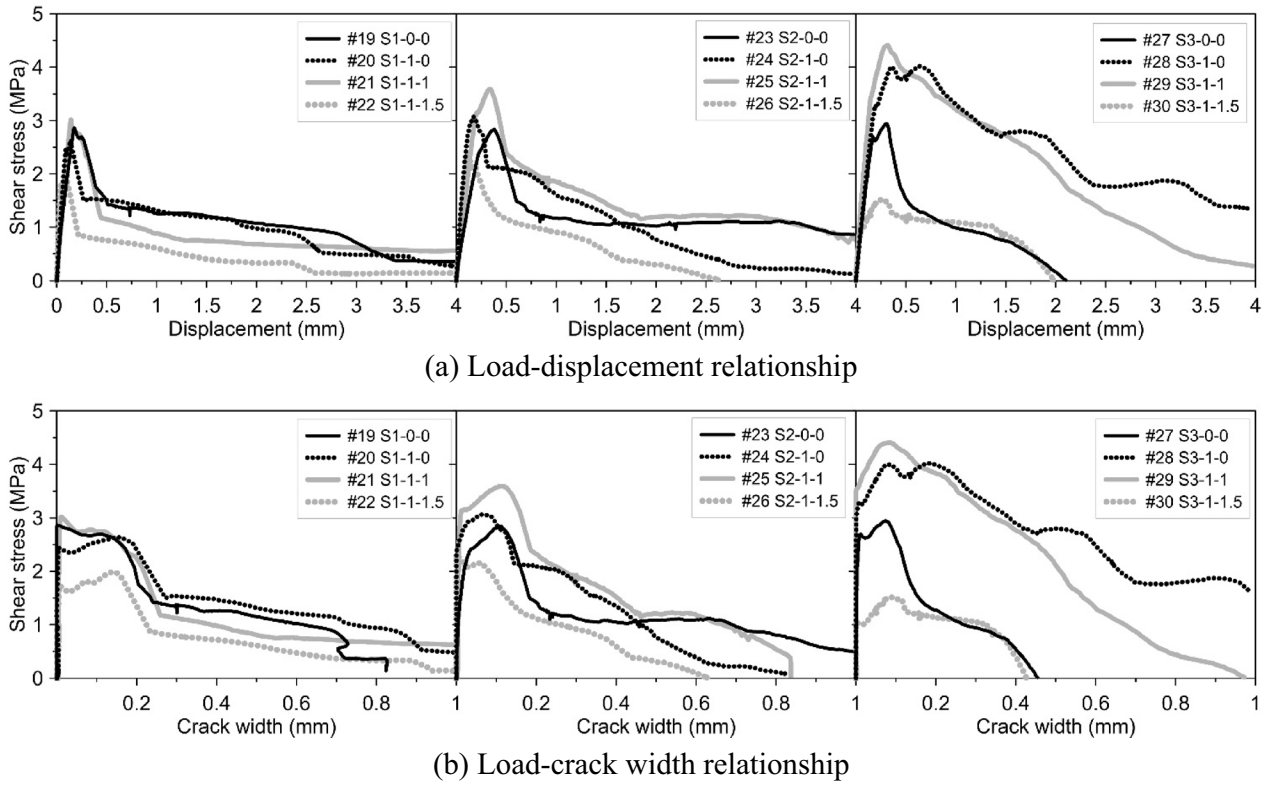

Fig. 11 Comparison of concrete contribution

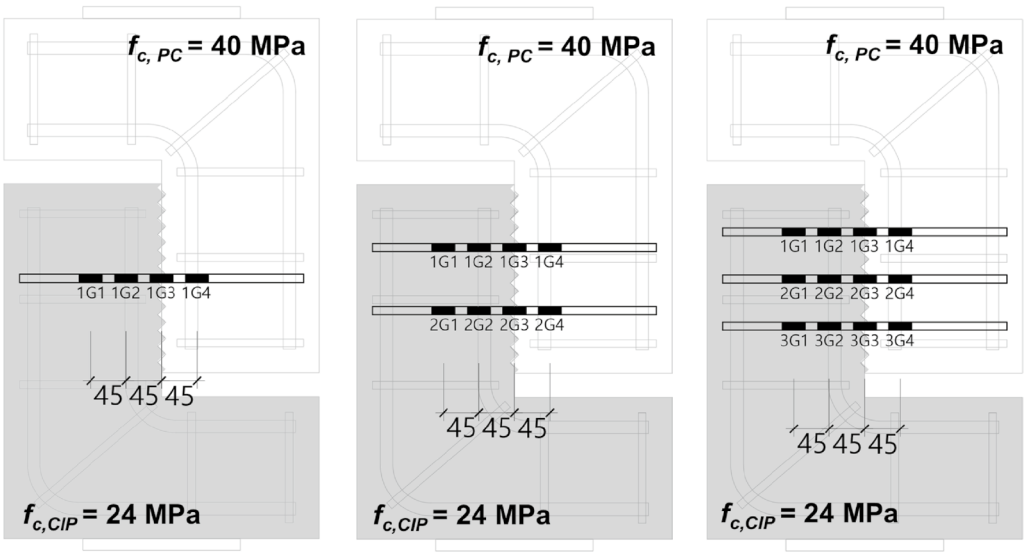

(a) S1 series (b) S2 series (c) S3 series

Fig. 12 Rebar strain location

strain at the interface in the 0–0 Series. This result is consistent with the findings of Kono et al. (2003).

Furthermore, previous research (Preti et al., 2023) reports that slip deformation and cracking of concrete occur due to the dowel action of the longitudinal reinforcement under shear force, which affects rebar yield penetration within the concrete block. Accordingly, the influence of dowel action was indirectly evaluated through the strain behavior of the concrete. As the steel fiber content increased, strain concentration at the interface due to the increased resistance to dowel action was observed, and the strain outside the interface was smaller than that at the interface compared to the 0–0 Series. Nonetheless, the strain in the reinforcement because dowel action was greater or at an equal level in the CIP part in most specimens. Dowel action increased with the inclusion of steel fibers, which is influenced by the tensile strength of the concrete, indicating that this effect should be considered.

5 Shear Friction Strength of SFRC Cast at Different Times

The actual shear friction strength of the specimens (v_u) was compared with the shear friction strength (v_n) calculated using current design codes. Fig. 14 compares the predicted values from various standards with the test results, with the estimates categorized into roughened and smooth interfaces. The coefficients used in the determination of design strength according to the standards are those presented in Chapter 2. The results are presented in Tables 7, 8, 9. Eurocode2, ModelCode 2020 (MC2020), and JSCE do not provide methods for calculating the shear friction strength of monolithically cast concrete. For specimens cast separately without reinforcement, EC2, MC2020, and AASHTO consider the contribution of concrete, whereas ACI 318-19 and JSCE do not. In this study, the results were categorized into specimens with and without reinforcement, and for specimens without reinforcement, the mean and coefficient of variation (C.O.V.) were not considered.

The average values of the shear friction strength ratio v_u/v_n showed that MC2020 had the highest range, from 1.599 to 1.940. ACI 318-19 followed with a range of 1.163 to 1.901, and EC2 ranged from 0.942 to 1.143. EC2 provided the closest estimate to 1.0, while MC2020 evaluated all interfaces on the conservative side, with relatively small differences between the values for different interfaces.

The coefficient of variation (C.O.V.) was the lowest for EC2 at 0.18, followed by AASHTO at 0.19, MC2020 at 0.26, and ACI at 0.33, indicating that EC2 had the narrowest distribution. EC2 incorporates the tensile strength of concrete in its design equation, and it was shown to accurately predict both the C.O.V. the shear friction strength ratio when considering the effect of concrete. Future studies should account for the effects of dowel action and interlocking in concrete when evaluating shear strength at the interface.

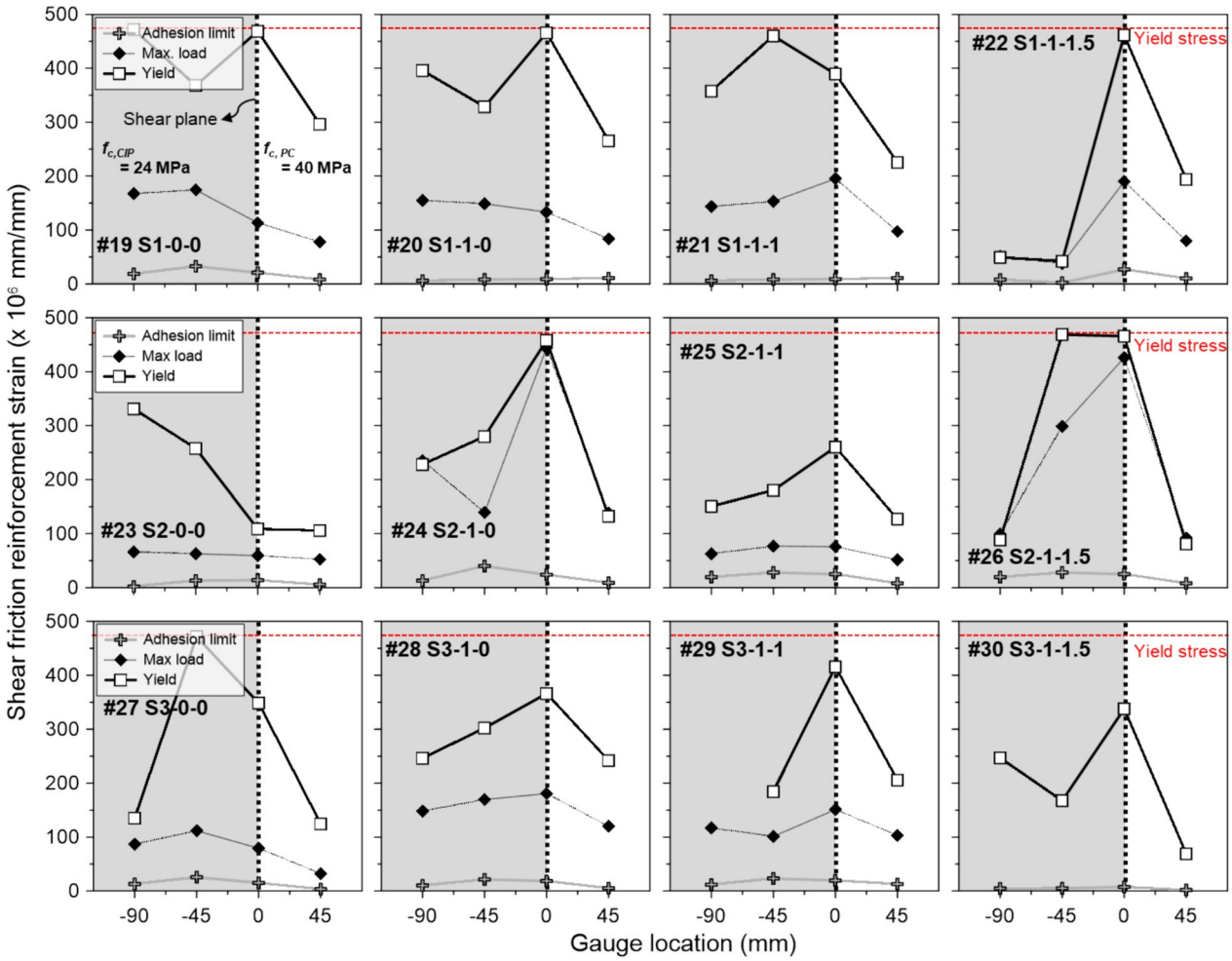

Fig. 13 Rebar strain distribution

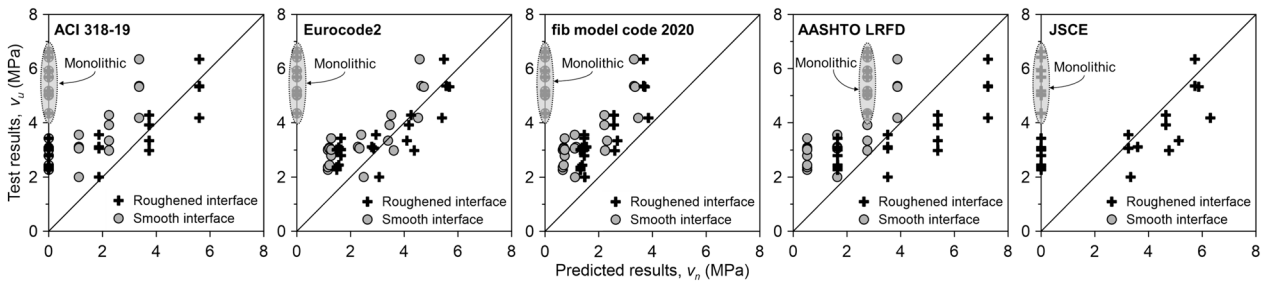

Fig. 14 Comparison of test results and predicted values

6 Conclusions

In this study, a total of 30 push-off tests were conducted to evaluate the shear friction mechanism and contribution of shear friction in both monolithically and separately cast steel fiber-reinforced concrete. The variables considered were casting method, steel fiber content, and the clamping force of the shear friction reinforcement. The conclusions are as follows:

1. The shear friction strength of monolithically cast concrete increased with the inclusion of steel fibers. Furthermore, with the enhanced ductility, additional

Table 7 Comparison of experimental results by current design code (monolithic and non-monolithic specimen without shear friction reinforcements)

No	Specimen ID	v_u (MPa)	ACI 318-19 KDS 14 20 22		Eurocode2		fib Model code 2020		AASHTO LRFD		JSCE	
			v_n (MPa)	v_u/v_n	v_n (MPa)	v_u/v_n	v_n (MPa)	v_u/v_n	v_n (MPa)	v_u/v_n	v_n (MPa)	v_u/v_n
1	M-24-0-a	5.01	0	–	–	–	–	–	2.76	1.817	–	–
2	M-24-0-b	5.17	0	–	–	–	–	–	2.76	1.875	–	–
3	M-24-1-a	6.62	0	–	–	–	–	–	2.76	2.402	–	–
4	M-24-1-b	5.92	0	–	–	–	–	–	2.76	2.147	–	–
5	M-24-1.5	6.42	0	–	–	–	–	–	2.76	2.326	–	–
6	M-40-0-a	5.04	0	–	–	–	–	–	2.76	1.828	–	–
7	M-40-0-b	4.35	0	–	–	–	–	–	2.76	1.576	–	–
8	M-40-1-a	5.68	0	–	–	–	–	–	2.76	2.060	–	–
9	M-40-1-b	5.68	0	–	–	–	–	–	2.76	2.060	–	–
10	S0-0-0-a	2.27	0	–	1.49	1.529	1.32	1.720	1.65	1.376	0	–
11	S0-0-0-b	2.37	0	–	1.49	1.595	1.32	1.794	1.65	1.435	0	–
12	S0-0-0-c	3.00	0	–	1.49	2.023	1.32	2.276	1.65	1.821	0	–
13	S0-1-0-a	2.44	0	–	1.56	1.567	1.39	1.763	1.65	1.481	0	–
14	S0-1-0-b	3.08	0	–	1.56	1.976	1.39	2.223	1.65	1.867	0	–
15	S0-1-0-c	3.05	0	–	1.56	1.953	1.39	2.197	1.65	1.845	0	–
16	S0-1-1-a	3.42	0	–	1.64	2.083	1.46	2.344	1.65	2.074	0	–
17	S0-1-1-b	2.79	0	–	1.64	1.700	1.46	1.912	1.65	1.692	0	–
18	S0-1-1-c	3.01	0	–	1.64	1.832	1.46	2.061	1.65	1.824	0	–

Table 8 Comparison of experimental results by current design code (non-monolithic specimen with shear friction reinforcements-roughened interface)

No	Specimen ID	v_u (MPa)	ACI 318-19 KDS 14 20 22		Eurocode2		fib Model code 2020		AASHTO LRFD		JSCE	
			v_n (MPa)	v_u/v_n	v_n (MPa)	v_u/v_n	v_n (MPa)	v_u/v_n	v_n (MPa)	v_u/v_n	v_n (MPa)	v_u/v_n
19	S1-0-0	3.11	1.87	1.665	2.79	1.113	1.54	2.020	3.52	0.884	3.60	0.864
20	S1-1-0	3.06	1.87	1.639	2.87	1.067	1.46	2.094	3.52	0.870	3.25	0.941
21	S1-1-1	3.55	1.87	1.903	2.95	1.205	1.46	2.432	3.52	1.010	3.25	1.093
22	S1-1-1.5	2.00	1.87	1.073	3.07	0.653	1.48	1.354	3.52	0.570	3.34	0.601
23	S2-0-0	3.34	3.73	0.893	4.10	0.814	2.69	1.238	5.38	0.620	5.13	0.651
24	S2-1-0	3.91	3.73	1.048	4.17	0.938	2.57	1.526	5.38	0.727	4.65	0.843
25	S2-1-1	4.28	3.73	1.146	4.26	1.006	2.57	1.668	5.38	0.795	4.65	0.921
26	S2-1-1.5	2.98	3.73	0.798	4.37	0.681	2.60	1.147	5.38	0.553	4.76	0.625
27	S3-0-0	4.18	5.60	0.746	5.41	0.773	3.85	1.085	7.25	0.576	6.30	0.663
28	S3-1-0	6.35	5.60	1.133	5.48	1.158	3.67	1.729	7.25	0.875	5.73	1.108
29	S3-1-1	5.36	5.60	0.957	5.56	0.963	3.67	1.460	7.25	0.739	5.73	0.936
30	S3-1-1.5	5.33	5.60	0.951	5.68	0.938	3.71	1.434	7.25	0.735	5.87	0.908
Mean		–	–	1.163	–	0.942	–	1.599	–	0.746	–	0.846
C.O.V		–	–	0.319	–	0.192	–	0.257	–	0.197	–	0.207

shear friction reinforcement may not be necessary for parts subject to direct shear in precast concrete members when steel fibers are used.

2. In the case of separately cast specimens, the strength improved with the inclusion of steel fibers, and the rate of strength increase also grew as the fiber content increased. In all specimens, the reinforcement did not yield at the point of maximum strength, and this mechanism should be considered when calculating shear friction strength.

Table 9 Comparison of experimental results by current design code (non-monolithic specimen with shear friction reinforcements-smooth interface)

No	Specimen ID	v_u (MPa)	ACI 318-19 KDS 14 20 22		Eurocode		fib Model code 2020		AASHTO LRFD	
			v_n (MPa)	v_u/v_n	v_n (MPa)	v_u/v_n	v_n (MPa)	v_u/v_n	v_n (MPa)	v_u/v_n
19	S1-0-0		1.12	2.830	2.28	1.366	1.16	2.688	1.64	1.898
20	S1-1-0		1.12	2.830	2.33	1.311	1.10	2.770	1.64	1.869
21	S1-1-1		1.12	3.160	2.40	1.482	1.10	3.217	1.64	2.170
22	S1-1-1.5		1.12	3.625	2.49	0.805	1.12	1.793	1.64	1.224
23	S2-0-0		2.24	1.415	3.40	0.982	2.31	1.443	2.76	1.210
24	S2-1-0		2.24	1.415	3.45	1.134	2.21	1.772	2.76	1.420
25	S2-1-1		2.24	1.580	3.52	1.217	2.21	1.937	2.76	1.552
26	S2-1-1.5		2.24	1.812	3.61	0.825	2.23	1.333	2.76	1.080
27	S3-0-0		3.36	0.943	4.52	0.925	3.47	1.204	3.88	1.077
28	S3-1-0		3.36	0.943	4.57	1.387	3.31	1.915	3.88	1.636
29	S3-1-1		3.36	1.053	4.64	1.155	3.31	1.617	3.88	1.382
30	S3-1-1.5		3.36	1.208	4.73	1.126	3.35	1.589	3.88	1.374
Mean		–	–	1.901	–	1.143	–	1.940	–	1.491
C.O.V		–	–	0.499	–	0.195	–	0.323	–	0.232

3. An evaluation of the shear strain according to the concrete mix proportion showed no significant difference between the 40 and 24 MPa concrete. Therefore, both concrete strengths contribute to resisting the load, and both should be considered in future research when designing for shear friction strength.
4. The evaluation of the contributions of shear friction reinforcement and concrete, based on shear transfer mechanism of AASHTO LRFD, revealed that, except for the group with 1.5% steel fibers, the concrete contribution increased with higher volume fraction of steel fiber. Additionally, the strain distribution in the reinforcement indicated that deformation due to dowel action was concentrated in the central region, suggesting that steel fibers improve dowel action, which is influenced by the tensile strength of the concrete.
5. Comparing the experimental results with predicted values from current design standards, Eurocode2, which considers the tensile strength of concrete, provided the closest match to 1.0, followed by ACI 318-19, fib Model Code 2020, and AASHTO LRFD. This suggests that the tensile strength increase due to steel fibers should be considered when using steel fiber-reinforced concrete. Future research should incorporate the effects of dowel action and interlocking in concrete into design considerations.

Acknowledgements
The authors acknowledge the financial support from National Research Foundation of Korea and Institute of Information & Communications Technology Planning & Evaluation

Author contributions
Daun Jeong: experimental data measurement, writing original draft preparation, investigation; Dong-Hee Son: conceptualization, methodology, experimental design, editing, reviewing; Chang-Sik Choi: supervision, validation, reviewing, editing; Baek-Il Bae: validation, reviewing and editing.

Funding
This research was supported by the Basic Science Research Program through the National Research Foundation of Korea (NRF) (NRF-2022R1A2C3008940, RS-2023-00207763) and Institute of Information & Communications Technology Planning & Evaluation (IITP) (RS-2020-II201373) grant funded by the Korean Government.

Availability of data and materials
All data generated or analyzed during this study are included in this published article.

Declarations

Ethics approval and consent to participate
Not applicable.

Consent for publication
The authors give consent to the publisher for publication.

Competing interests
The authors declare no competing interests.

Received: 19 September 2024 Accepted: 25 December 2024
Published online: 17 April 2025

References

Abbas, S., Soliman, A. M., & Nehdi, M. L. (2014). Mechanical performance of reinforced concrete and steel fiber-reinforced concrete precast tunnel lining segments: A case study. *ACI Materials Journal*. https://doi.org/10.14359/51687101

ACI Committee 544. (2002). *State of the art report on fiber reinforced concrete (5441R-96)*. American Concrete Institute.

Barragan, B., Gettu, R., Agullo, L., & Zerbino, R. (2006). Shear failure of steel fiber-reinforced concrete based on push-off tests. *ACI Materials Journal, 103*(4), 251. https://doi.org/10.14359/16608

Birkeland, P. W., & Birkeland, H. W. (1966). Connections in precast concrete construction. *ACI Structural Journal, 63*(3), 345–368. https://doi.org/10.14359/7627

Hanson, N. W. (1960). Precast-prestressed concrete bridges 2: Horizontal shear connections. *Journal of the PCA Research and Development Laboratories, 17*(4), 38–58.

Harries, K. A., Zeno, G., & Shahrooz, B. (2012). Toward an improved understanding of shear-friction behavior. *ACI Structural Journal, 109*(6), 835–844. https://doi.org/10.14359/51684127

Hsu, T. T. C., Mau, S. T., & Chen, B. (1987). Theory of shear transfer strength of reinforced concrete. *ACI Structural Journal, 84*(2), 149–160. https://doi.org/10.14359/2834

Jang, H., Lee, H., Cho, K., & Kim, J. (2017). Experimental study on shear performance of plain construction joints integrated with ultra-high performance concrete (UHPC). *Construction and Building Materials, 152*, 16–23. https://doi.org/10.1016/j.conbuildmat.2017.06.156

Kahn, L. F., & Mitchell, A. D. (2002). Shear friction tests with high-strength concrete. *ACI Structural Journal, 99*(1), 98–103. https://doi.org/10.14359/11040

Kal, K., Kim, K., Lee, D., Hwang, J., & Oh, Y. (2010). Experimental study on shear strength of steel fiber reinforced concrete beams. *Journal of the Korea Institute for Structural Maintenance and Inspection, 14*(3), 160–170.

Kono, S., Tanaka, H., & Watanabe, F. (2003). Interface shear transfer for high strength concrete and high strength shear friction reinforcement. *In High performance materials in bridges*, pp 319–328. https://doi.org/10.1061/40691(2003)28

Lee, J. H., Kim, H. Y., & Lee, B. S. (2019). Shear friction behavior of RC members with high strength and large diameter steel bars. *Journal of the Korea Concrete Institute, 31*(6), 577–587. https://doi.org/10.4334/JKCI.2019.31.6.577

Loov, R. E., & Patnaik, A. K. (1994). Horizontal shear strength of composite concrete beams with a rough interface. *PCI Journal, 39*(1), 48–69. https://doi.org/10.15554/pcij.01011994.48.69

Martin, L. D., & Perry, C. J. (Eds.). (2004). *PCI design handbook: Precast and prestressed concrete*. Precast/Prestressed Concrete Institute.

Mast, R. F. (1968). Auxiliary reinforcement in precast concrete connections. *ASCE Journal of the Structural Division, 94*(6), 1485–1504. https://doi.org/10.1061/JSDEAG.0001977

Mattock, A. H., & Hawkins, N. M. (1972). Shear transfer in reinforced concrete—recent research. *PCI Journal, 17*(2), 55–75. https://doi.org/10.15554/pcij.03011972.55.75

Picazo, A., Alberti, M. G., Gálvez, J. C., & Enfedaque, A. (2021). Shear slip post-cracking behaviour of polyolefin and steel fibre reinforced concrete. *Construction and Building Materials, 290*, 123187. https://doi.org/10.1016/j.conbuildmat.2021.123187

Preti, M., Paderno, A., & Cominoli, L. (2023). Dowel behaviour of rebars under combined axial and shear actions. *Materials and Structures, 56*(5), 93. https://doi.org/10.1617/s11527-023-02182-0

Randi, N. (2007). Load bearing behaviour of cast-in shear dowels. *Belon- und Stahlhetonhau, 102*(Special Edition), 31–37. https://doi.org/10.1002/best.200710103

Randi, N. (2013). Design recommendations for interface shear transfer in fib Model Code 2010. *Structural Concrete, 14*(3), 230–241. https://doi.org/10.1002/suco.201300003

Resende, T. L., Cardoso, D. C., & Shehata, L. C. (2020). Influence of steel fibers on the dowel action of RC beams without stirrups. *Engineering Structures, 221*, 111044. https://doi.org/10.1016/j.engstruct.2020.111044

Sagi, M. S. V., Lakavath, C., & Prakash, S. S. (2022). Effect of steel fibers on the shear behavior of Self-Compacting reinforced concrete deep Beams: An experimental investigation and analytical model. *Engineering Structures, 269*, 114802. https://doi.org/10.1016/j.engstruct.2022.114802

Semendary, A. A., Hamid, W. K., Steinberg, E. P., & Khoury, I. (2020). Shear friction performance between high strength concrete (HSC) and ultra high performance concrete (UHPC) for bridge connection applications. *Engineering Structures, 205*, 110122. https://doi.org/10.1016/j.engstruct.2019.110122

Soetens, T., & Matthys, S. (2017). Shear-stress transfer across a crack in steel fibre-reinforced concrete. *Cement and Concrete Composites, 82*, 1–13. https://doi.org/10.1016/j.cemconcomp.2017.05.010

Son, D. H., Bae, B. I., & Choi, C. S. (2022). Shear strength evaluation of diagonally reinforced concrete coupling beams with steel fibers. *ACI Structural Journal*. https://doi.org/10.14359/51734525

Son, D. H., Bae, B. I., Lee, J., & Choi, C. S. (2024a). Shear strength of steel fiber reinforced concrete exterior beam-column joints with various anchorage details under cyclic loading. *Structures, 61*, 105940.

Son, D. H., Choi, J. Y., Song, S., Choi, C. S., & Bae, B. I. (2024b). Inelastic behavior of diagonally reinforced coupling beams confined with steel fibers. *Structures, 65*, 106733. https://doi.org/10.1016/j.istruc.2024.106733

Vecchio, F. J., & Collins, M. P. (1986). The modified compression-field theory for reinforced concrete elements subjected to shear. *ACI Structural Journal, 83*(2), 219–231. https://doi.org/10.14359/10416

Zhang, Y., Liu, A., Chen, B., Zhang, J., Pi, Y. L., & Bradford, M. A. (2020). Experimental and numerical study of shear connection in composite beams of steel and steel-fibre reinforced concrete. *Engineering Structures, 215*, 110707. https://doi.org/10.1016/j.engstruct.2020.110707

Publisher's Note

Daun Jeong Graduate student, Department of Architectural Engineering, Hanyang University, 222, Wangsimni-ro, Seongdong-Gu, Seoul 04763, Republic of Korea.

Dong-Hee Son Postdoctoral researcher, Department of Architectural Engineering, Hanyang University, 222, Wangsimni-ro, Seongdong-Gu, Seoul 04763, Republic of Korea.

Chang-Sik Choi Professor, Department of Architectural Engineering, Hanyang University, 222, Wangsimni-ro, Seongdong-Gu, Seoul 04763, Republic of Korea.

Baek-Il Bae Professor, Department of Digital Architecture and Urban Engineering, Hanyang Cyber University, 220, Wangsimni-ro, Seongdong-Gu, Seoul 04763, Republic of Korea.